



IMPLEMENTATION OF ACTUATING DEVICES TO CONTROL/IDENTIFY STRUCTURES

Jong-Cheng Wu¹

ABSTRACT

The use of structural control for the mitigation of natural hazards such as earthquakes and hurricanes toward mature implementation requires thorough understanding in the integrated behavior of the structure and active devices (actuators). For wind-excited structures, the wind tunnel experiments with active control provide the best way of gaining the information of such a behavior and accumulating implementation experiences in the wind engineering application. This paper emphasizes the importance and presents the concept of a suitable design process for active control application. This approach provides the capability of taking into account the possible control-structure interaction and aeroelasticity. The results of a successful implementation of using the active mass driver (AMD) system on a 1/300 scaled multiple-degree-of-freedom high-rise building model through wind tunnel tests is used to demonstrate its applicability. Several important issues such as the identification scheme, the construction of nominal system for controller design and the requirements in the actuator specifications will be addressed from the practical point of view. Advanced control strategies, including the LQG (linear quadratic gaussian) method and the idea of robust H_∞ control using LMI (linear matrix inequality) approach for an uncertain system, are investigated and verified in the experiments. Meanwhile, based on the experiences of implementing actuators in the active control, the experimental studies on wind-structure interaction are conducted by using actuating devices. The conceptual idea and the examples of on-going projects for identifying wind-structure interaction via forced excitation are introduced.

Keywords: Actuating Devices, Linear Matrix Inequality (LMI), H_∞ Control, Linear Quadratic Gaussian (LQG), Wind Tunnel Tests

1. INTRODUCTION

Over the last decade, many research and industrial efforts [e.g., Housner *et al.* (1994), Kobori *et al.* (1998), Casciati (2002)] have demonstrated that the use of structural active control provides an excellent alternative for vibration suppression of civil structures during the attack of natural hazards such as earthquakes and hurricanes (typhoons). As the progress of employing control technique has largely come to the stage of actual implementation other than just numerical investigation in the interest of research, several issues surrounding the integration of active device (actuator) with the structure would have to be addressed. It is well understood that the thorough knowledge of these issues serve a better solution in obtaining good performance in implementation.

The 1st issue accompanying such an integration problem, the so-called control-structure interaction (CSI), was firstly systematically investigated by [Dyke *et al.* (1995, 1996)] on a scaled model and later confirmed by [Wu (2000)] using a full-scale experimental building. For instance, shown in Figs. 1-3 are illustrations of CSI effect of a full-scale 3-story building model presented in [Wu (2000)]. The building shown in Fig. 1 has a total weight of about 30 tons, roughly equally shared by each floor. An active bracing system (ABS) that is composed of a steel bracing and an actuator is equipped at the first

¹ Professor, Department of Civil Engineering, Tamkang University, Taipei, Taiwan, joncheng@mail.tku.edu.tw

floor of the building. Figs. 2 and 3 demonstrate the actuator performance, i.e., its transfer function of actuating force versus control command, before and after installation of the actuator to the structure. It is observed that due to the CSI effect, the transfer function of the actuator is no longer characterized by a simple time delay but a more complex dynamics. In fact, it shows that it is difficult for the actuator to generate active force at the frequencies of structural modes. This means the consideration of CSI effect in implementation is inevitable, especially for implementation with a large scale. In the aspect of control application to wind engineering, the same conclusion shall apply regardless of the difference of excitation sources.



Fig. 1: 3-Story Full-Scale Building Model

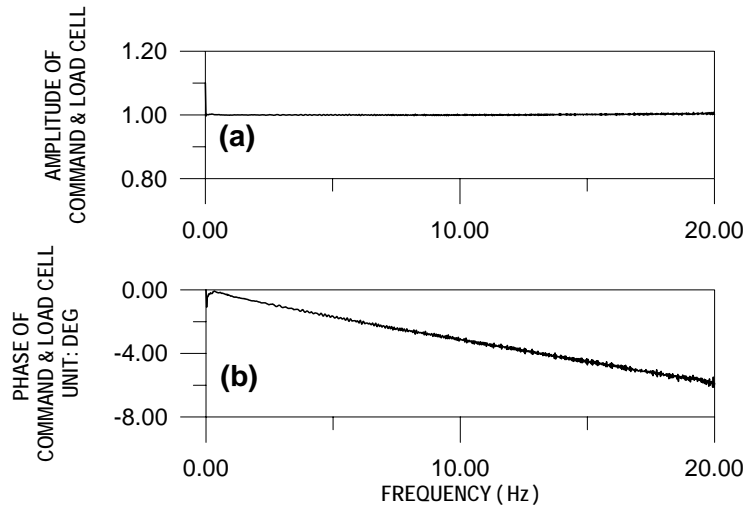


Fig. 2: Transfer Function of Actuator before Installation; (a) Amplitude, and (b) Phase Angle

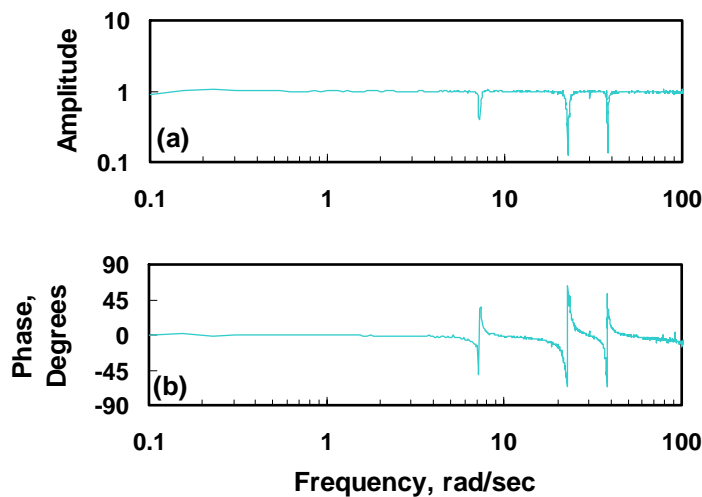


Fig. 3: Transfer Function of Actuator after Installation; (a) Amplitude, and (b) Phase Angle

According to the previous statement, the 2nd issue to be addressed in implementation is the suitable design process in active control, which can take into account such a control-integrated effect. Notably, the identification scheme actually plays the key role in the design process and its importance should be emphasized to ensure good performance in implementation. For wind-excited structures, the implementation of active control using wind tunnel tests provides the best way to gain the information

on such an integrated effect and serves as the most convincing approach in verifying the appropriate design process toward mature application in the wind engineering.

This paper proposes the general concept of a suitable design process in active control, which involves a feasible identification scheme to take into account the CSI effect and the possible wind-structure interaction, the so-called aeroelasticity, as well. The example of a successful implementation using an active mass driver (AMD) system on a 1/300 scaled multiple-degree-of-freedom high-rise building model in the wind tunnel is used to demonstrate its applicability. This paper also discusses other issues such as the idea of robust control and the requirements in the actuator specification. Aside from these, based on the experiences of implementing actuators in the active control, the experimental studies on wind-structure interaction by using actuating devices become possible. The general concept and the examples of on-going projects for identifying wind-structure interaction via forced excitation are also briefly introduced.

2. GENERAL CONCEPT OF A SUITABLE DESIGN PROCESS

2.1 Identification Scheme

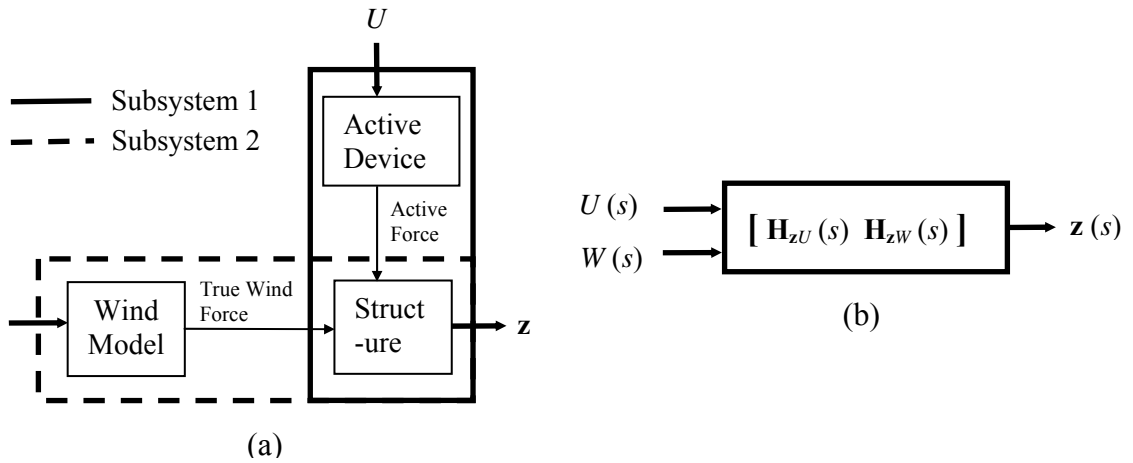


Fig.4: (a) Schematic Block Diagram of the Control-Integrated Wind-Excited System; (b) Overall Block Diagram in Laplace Domain.

The identification scheme is the key element in the design process for active control. To take care of the CSI effect and aeroelasticity mentioned previously, a proper identification scheme is proposed in the form of block diagram as shown in Fig. 4(a). In this block diagram, the response vector z (termed as the controlled output) in the control-integrated wind-excited system is regarded as the superposition of two subsystems excited by two respective input sources: the control command U and the fictitious wind load W . The subsystem 1 has the control command U as the input and the response z as the output, therefore it should contain the integrated dynamics of the active device and the structure, i.e., the possible CSI effect. On the other hand, the true wind force (see Fig. 4(a)) is resulted from the wind blow that might contain aeroelasticity. To take the aeroelasticity into account, the subsystem 2 should contain not only the structure itself but also a wind model acting as the intermediate block that has the fictitious wind load W as its input. Technically, W can be treated as a white noise with unity spectrum for simplicity. Fig. 4(b) shows the transfer function relation of the block diagram in Laplace domain, in which $\mathbf{H}_{zU}(s)$ and $\mathbf{H}_{zW}(s)$ represent the transfer function from U to z and that from W to z , respectively.

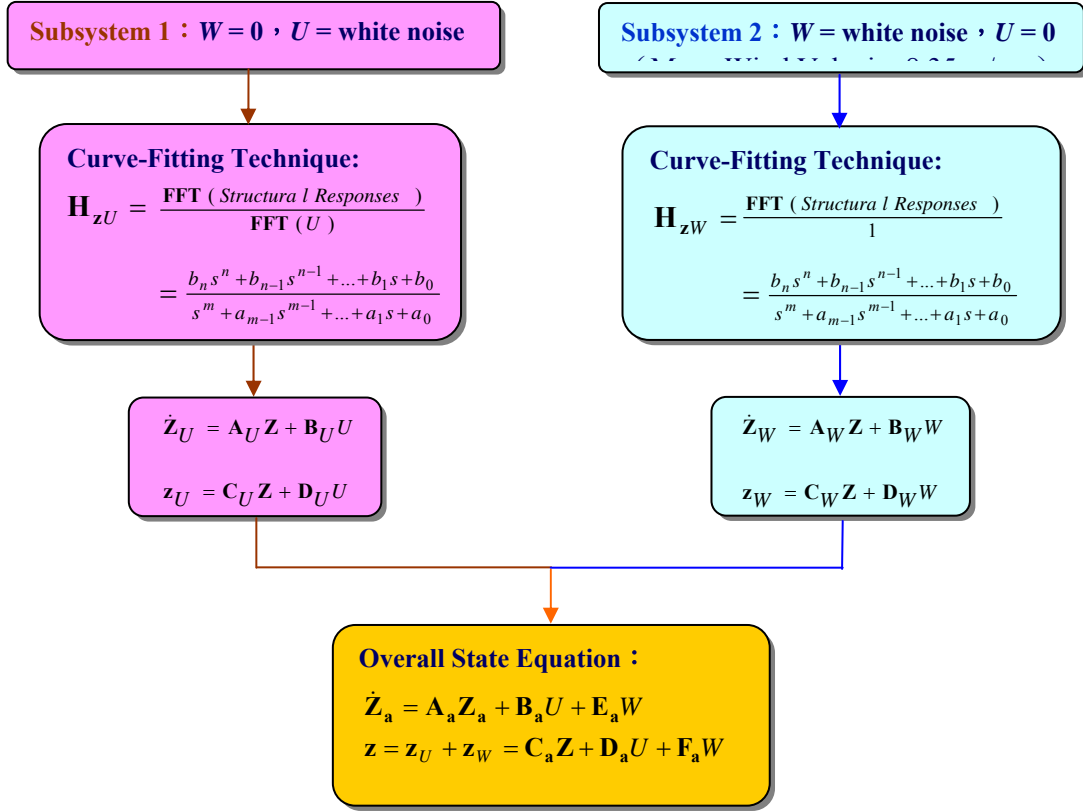


Fig. 5: Schematic Flow of Identification

By considering the excitation of the individual input U or W , each subsystem can be identified and their state space equations can be constructed based on the curve-fitting results of measured frequency response functions. Readers interested in the curve-fitting technique can refer to [Wu and Pan (2002), Wu (2000)] for the detailed information. The state equations of $H_{zU}(s)$ and $H_{zW}(s)$ thus obtained are expressed as

$$\dot{z}_U = A_U z_U + B_U U \quad ; \quad z_U = C_U z_U + D_U U \quad (1)$$

and

$$\dot{z}_W = A_W z_W + B_W W \quad ; \quad z_W = C_W z_W + D_W W \quad (2)$$

, respectively. Both equations are then cast together to yield the overall system with the state equation expressed by

$$\dot{z}_a = A_a z_a + B_a U + E_a W \quad ; \quad z = z_U + z_W = C_a z + D_a U + F_a W \quad (3)$$

in which

$$\mathbf{z}_a = \begin{bmatrix} \mathbf{z}_U \\ \mathbf{z}_W \end{bmatrix}; \mathbf{A}_a = \begin{bmatrix} \mathbf{A}_U & 0 \\ 0 & \mathbf{A}_W \end{bmatrix}; \mathbf{B}_a = \begin{bmatrix} \mathbf{B}_U \\ 0 \end{bmatrix}; \mathbf{E}_a = \begin{bmatrix} 0 \\ \mathbf{B}_W \end{bmatrix}; \mathbf{C}_a = [\mathbf{C}_U \quad \mathbf{C}_W]; \mathbf{D}_a = \mathbf{D}_U; \quad (4)$$

$$\mathbf{F}_a = \mathbf{D}_W$$

The schematic flow of identification is illustrated in Fig. 5.

In general, aeroelasticity in wind-excited flexible structures is likely to occur. However, for most high-rise buildings, the basic aerodynamic loading induced in the along-wind direction is a wide-banded spectrum due to buffeting, while that induced in the across-wind direction is a narrow-banded spectrum caused by the vortex shedding effect [Simiu and Scanlan (1996)]. Unless the so-called lock-in behavior occurs, the aeroelasticity involved is usually not significant. In such cases, the wind model in the block of subsystem 2 can be explicitly identified. The spectrum of true wind force can be obtained directly from the wind load data acquired from the high frequency force-balance test of an

aerodynamic model. The examples of identification in either way will be demonstrated by the high-rise building model presented in the later section.

2.2 Plant System

The overall state equation of Eq. (3) obtained from identification may contain uncontrollable or unobservable modes induced from direct superposition of the two subsystem systems. In most circumstances, it is necessary to reduce the overall system to the minimal system. Though there are many methods for system reduction, it is suggested that the balanced state reduction method proposed in [Moore (1981)] is a promising method because it guarantees the same controllability and observability after reduction. The minimal system denoted by $(\mathbf{A}_p, \mathbf{B}_p, \mathbf{C}_p, \mathbf{D}_p, \mathbf{E}_p, \mathbf{F}_p)$ with smaller state \mathbf{Z}_p thus obtained can be denoted as the plant system $\mathbf{P}(s)$ and ready to be used for the design of controllers.

2.3 Nominal System and Control Methods

The nominal system is a system that the controller is designed based on. To design a simpler controller such as LQG (linear quadratic gaussian) controller, the plant system is directly used as the nominal system. In such a case, the control block diagram is shown in Fig. 6, in which \mathbf{y} is the measured output that is to be used as the feedback quantities. The measured output \mathbf{y} can be extracted from the controlled output \mathbf{z} in Eq. (3). In Fig. 6, the block $\mathbf{K}(s)$ is the controller system to be designed. Based on the assumption that the excitation W and the measurement noise \mathbf{v} are uncorrelated Gaussian white noise processes, the objective of a LQG controller is to minimize the performance index function defined by

$$J = \lim_{\tau \rightarrow \infty} \frac{1}{\tau} \mathbf{E} \left\{ \int_0^\tau (\bar{\mathbf{z}}' \mathbf{Q} \bar{\mathbf{z}} + U' R U) dt \right\} \quad (5)$$

in which $\bar{\mathbf{z}} = \mathbf{z} - \mathbf{F}_p W = \mathbf{C}_p \mathbf{Z}_p + \mathbf{D}_p U$, and \mathbf{Q} and R are weighting matrices. The detailed formulation of LQG control can be found in [Wu (2000)].

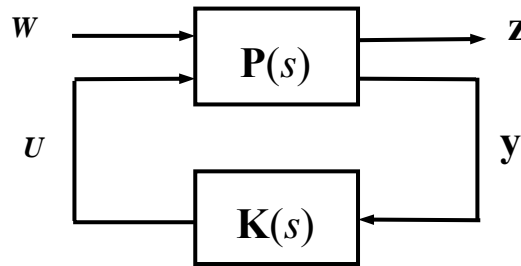


Fig. 6 : Block Diagram of LQG Control

In fact, a more mature controller design requires the consideration of performance robustness and stability robustness, as is emphasized by many modern control theories. In this aspect, the idea of H_∞ control is particularly useful because the robustness requirements can be interpreted as the H_∞ norm of a transfer function matrix smaller than an attenuation value [Zhou and Doyle (1998)]. The recent progress of the numerical tool of linear matrix inequality (LMI) has even facilitated its solution procedure that makes the H_∞ control theory more concise and straightforward.

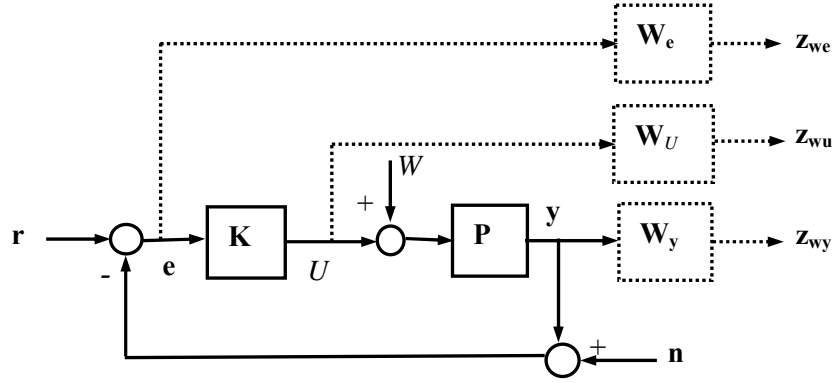


Fig. 7: Block Diagram of Wind-excited Civil Structure with Active Control

One example of applying H_∞ control to the civil structure is stated in the following. The block diagram of a wind-excited civil structure with output-feedback control can be constructed as shown in Fig. 7 by the solid line portion. In Fig. 7, \mathbf{P} is the plant system; \mathbf{K} is the controller system; \mathbf{r} is the reference signal, U is the control command generated from the controller; W is the wind loading, \mathbf{n} is the measurement noise; \mathbf{y} is the measured output; and \mathbf{e} is the error signal that is the subtraction between the measured output and the reference signal. Herein the reference signal is taken as $\mathbf{r} = 0$ because vibration suppression is the concern. The measured output \mathbf{y} is taken from among the elements in the controlled output \mathbf{z} . From the robust control theory, the robustness requirements, namely, the performance robustness in terms of tracking error, disturbance attenuation and noise rejection, and stability robustness with respect to system uncertainty [Zhou and Doyle (1998)] can be converted from the block diagram in Fig. 7 into a standard H_∞ control problem as shown in Fig. 8. In Fig. 8, $\mathbf{G}(s)$ is the generalized nominal system. In other words, to satisfy the robustness requirements is equivalent to find a controller $\mathbf{K}(s)$ for the generalized nominal system $\mathbf{G}(s)$, under the proper choice of weighting matrices \mathbf{W}_e , \mathbf{W}_U and \mathbf{W}_y , such that $\|\mathbf{H}_{z_\infty d}\|_\infty < \gamma$, γ is the so-called attenuation value. The notation $\mathbf{H}_{z_\infty d}$ represents the transfer function from \mathbf{d} to \mathbf{z}_∞ with $\mathbf{z}_\infty = [\mathbf{z}_{we}^T \quad \mathbf{z}_{wu}^T \quad \mathbf{z}_{wy}^T]^T$ being the generalized controlled output and $\mathbf{d} = [\mathbf{r}^T \quad W^T]^T$ being the generalized exogenous input. It is noted that \mathbf{z}_{we} , \mathbf{z}_{wu} and \mathbf{z}_{wy} in \mathbf{z}_∞ are actually the weighted \mathbf{e} , U and \mathbf{y} , respectively, as shown by the dotted line portion in Fig. 7. The construction of the state equation for the generalized nominal system $\mathbf{G}(s)$ is described in the following.

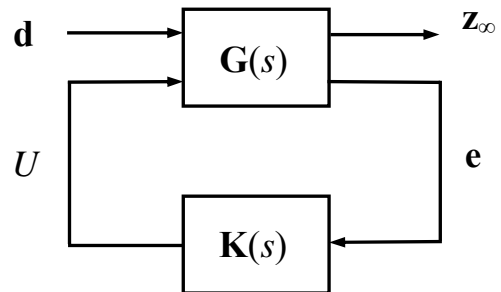


Fig. 8: Block Diagram of Standard H_∞ Control

In Fig. 7, the state equations of the plant system $\mathbf{P}(s)$, weightings $\mathbf{W}_e(s)$, $\mathbf{W}_U(s)$ and $\mathbf{W}_y(s)$ can be expressed as

$$\dot{\mathbf{Z}}_P = \mathbf{A}_P \mathbf{Z}_P + \mathbf{B}_P \mathbf{W} + \mathbf{E}_P U \quad ; \quad \mathbf{y} = \mathbf{C}_P \mathbf{Z}_P + \mathbf{D}_P \mathbf{W} + \mathbf{F}_P U \quad (6)$$

$$\dot{\mathbf{Z}}_{we} = \mathbf{A}_{we} \mathbf{Z}_{we} + \mathbf{B}_{we} \mathbf{e} \quad ; \quad \mathbf{z}_{we} = \mathbf{C}_{we} \mathbf{Z}_{we} + \mathbf{D}_{we} \mathbf{e} \quad (7)$$

$$\dot{\mathbf{Z}}_{wu} = \mathbf{A}_{wu} \mathbf{Z}_{wu} + \mathbf{B}_{wu} U \quad ; \quad \mathbf{z}_{wu} = \mathbf{C}_{wu} \mathbf{Z}_{wu} + \mathbf{D}_{wu} U \quad (8)$$

$$\dot{\mathbf{Z}}_{wy} = \mathbf{A}_{wy} \mathbf{Z}_{wy} + \mathbf{B}_{wy} \mathbf{y} \quad ; \quad \mathbf{z}_{wy} = \mathbf{C}_{wy} \mathbf{Z}_{wy} + \mathbf{D}_{wy} \mathbf{y} \quad (9)$$

, respectively, in which \mathbf{Z}_P , \mathbf{Z}_{we} , \mathbf{Z}_{wu} , \mathbf{Z}_{wy} are the state vectors; \mathbf{A}_P , \mathbf{B}_P , \mathbf{C}_P , \mathbf{D}_P , \mathbf{E}_P , \mathbf{F}_P , \mathbf{A}_{we} , \mathbf{B}_{we} , \mathbf{C}_{we} , \mathbf{D}_{we} , \mathbf{A}_{wu} , \mathbf{B}_{wu} , \mathbf{C}_{wu} , \mathbf{D}_{wu} , \mathbf{A}_{wy} , \mathbf{B}_{wy} , \mathbf{C}_{wy} and \mathbf{D}_{wy} are constant matrices with appropriate dimensions. By considering \mathbf{r} and W as the exogenous input \mathbf{d} ; \mathbf{z}_{we} , \mathbf{z}_{wu} and \mathbf{z}_{wy} as the generalized controlled output; and \mathbf{e} as the generalized measured output, the generalized nominal system $\mathbf{G}(s)$ in Fig. 8 can be written as the state equations expressed by

$$\dot{\mathbf{Z}} = \mathbf{A} \mathbf{Z} + \mathbf{B}_1 \mathbf{d} + \mathbf{B}_2 U \quad ; \quad \mathbf{z}_\infty = \mathbf{C}_1 \mathbf{Z} + \mathbf{D}_{11} \mathbf{d} + \mathbf{D}_{12} U \quad ; \quad \mathbf{e} = \mathbf{C}_2 \mathbf{Z} + \mathbf{D}_{21} \mathbf{d} + \mathbf{D}_{22} U \quad (10)$$

in which

$$\mathbf{Z} = \begin{bmatrix} \mathbf{Z}_P \\ \mathbf{Z}_{we} \\ \mathbf{Z}_{wu} \\ \mathbf{Z}_{wy} \end{bmatrix} \quad ; \quad \mathbf{d} = \begin{bmatrix} \mathbf{r} \\ W \end{bmatrix} \quad ; \quad \mathbf{z}_\infty = \begin{bmatrix} \mathbf{z}_{we} \\ \mathbf{z}_{wu} \\ \mathbf{z}_{wy} \end{bmatrix} \quad ; \quad \mathbf{A} = \begin{bmatrix} \mathbf{A}_P & 0 & 0 & 0 \\ -\mathbf{B}_{we} \mathbf{C}_P & \mathbf{A}_{we} & 0 & 0 \\ 0 & 0 & \mathbf{A}_{wu} & 0 \\ \mathbf{B}_{wy} \mathbf{C}_P & 0 & 0 & \mathbf{A}_{wy} \end{bmatrix} \quad ;$$

$$\mathbf{B}_1 = \begin{bmatrix} 0 & \mathbf{B}_P \\ \mathbf{B}_{we} & -\mathbf{B}_{we} \mathbf{D}_P \\ 0 & 0 \\ 0 & \mathbf{B}_{wy} \mathbf{D}_P \end{bmatrix} \quad ; \quad \mathbf{B}_2 = \begin{bmatrix} \mathbf{E}_P \\ -\mathbf{B}_{we} \mathbf{F}_P \\ \mathbf{B}_{wu} \\ \mathbf{B}_{wy} \mathbf{F}_P \end{bmatrix} \quad ; \quad \mathbf{C}_1 = \begin{bmatrix} -\mathbf{D}_{we} \mathbf{C}_P & \mathbf{C}_{we} & 0 & 0 \\ 0 & 0 & \mathbf{C}_{wu} & 0 \\ \mathbf{D}_{wy} \mathbf{C}_P & 0 & 0 & \mathbf{C}_{wy} \end{bmatrix} \quad ; \quad (11)$$

$$\mathbf{D}_{11} = \begin{bmatrix} \mathbf{D}_{we} & -\mathbf{D}_{we} \mathbf{D}_P \\ 0 & 0 \\ 0 & \mathbf{D}_{wy} \mathbf{D}_P \end{bmatrix} \quad ; \quad \mathbf{D}_{12} = \begin{bmatrix} -\mathbf{D}_{we} \mathbf{F}_P \\ \mathbf{D}_{wu} \\ \mathbf{D}_{wy} \mathbf{F}_P \end{bmatrix} \quad ; \quad \mathbf{C}_2 = [-\mathbf{C}_P \quad 0 \quad 0 \quad 0] \quad ; \quad \mathbf{D}_{21} = [\mathbf{I} \quad -\mathbf{D}_P] \quad ;$$

$$\mathbf{D}_{22} = -\mathbf{F}_P$$

in which $\mathbf{e} = -\mathbf{y}$ is generalized measured output used as the feedback quantities.

The solution procedure of LMI approach in computing the H_∞ control problem with output feedback shown in Fig. 8 can be found in many literatures [e.g., Gahinet (1992), Gahinet *et al.* (1994), Scherer *et al.* (1997), Chilali *et al.* (1996)]. In the implemented example to be presented later, a simpler version of LMI approach proposed by [Gahinet (1992)] will be used.

The final form of the dynamic output feedback controller can be expressed as

$$\dot{\mathbf{q}} = \mathbf{A}_c \mathbf{q} + \mathbf{B}_c \mathbf{y} \quad ; \quad U = \mathbf{C}_c \mathbf{q} + \mathbf{D}_c \mathbf{y} \quad (12)$$

in which \mathbf{q} is a state vector to be computed in real time from the measured output \mathbf{y} , and \mathbf{A}_c , \mathbf{B}_c , \mathbf{C}_c , \mathbf{D}_c are constant matrices obtained from the controller design.

2.4 Discretization of Controllers

For implementation in real time, the dynamic output feedback controller, Eq. (12), should be further discretized into a discrete form with a proper sampling rate, i.e.,

$$\mathbf{q}(n+1) = \mathbf{A}_d \mathbf{q}(n) + \mathbf{B}_d \mathbf{y}(n) \quad ; \quad U(n) = \mathbf{C}_d \mathbf{q}(n) + \mathbf{D}_d \mathbf{y}(n) \quad (13)$$

To achieve this, a simple conversion by the bilinear transformation [Paraskevopoulos (1996)] is suggested. In Eq. (13), the index n and $n+1$ represent the present time instant and the next time instant, respectively.

3. REQUIREMENTS IN ACTUATOR SPECIFICATIONS

In the regard of performance in active control, the active devices (actuators) play the most significant role since it is the mechanism providing the actuating force to the structure for vibration suppression. Maximum capacity and frequency range of reaction are the two basic key elements that should be specified in the actuator characteristics. The frequency range of reaction depends on the range of frequency in the structural response that is to be controlled. In general, the control for accelerations requires higher frequency range of reaction since the structural acceleration contains more contribution from higher modes. For most high-rise buildings, the frequency range of reaction required up to the first two or at most three modes is expected to be satisfactory. As for the estimation of the maximum capacity, the numerical simulation can indicate a rough result as an initial reference.

In case that the control-structure interaction is significant, the choices of these two elements can not be justified until the active device is actually implemented. Due to the CSI effect, they may be degraded from the estimation. It is observed that, by following the identification suggested herein, the performance of active control can roughly reveal itself by calculating the ratio of the structural response excited by the actuator in maximum power (subsystem 1) versus that excited by the wind loads (subsystem 2).

4. EXAMPLES OF IMPLEMENTATION VIA WIND TUNNEL TESTS

A 4 degree-of-freedom shear type scaled building model that represents the 76-story wind-excited benchmark building proposed by the ASCE structural control committee is constructed and equipped with an active driver (AMD) system on the top degree-of-freedom. The model configuration and structural parameters are scaled down by the scaling factor 1:300 in length, 1:6 velocity, and 1:1 in density (accordingly, 1:50 in time). As shown in Fig.9 (a) is the frame skeleton of the scaled building model. The completed model with the attached exterior walls on the atmospheric boundary layer wind tunnel as shown in Fig. 9 (b) has a height/width ratio of 6.4 that is susceptible to wind disturbance. A pitot tube is installed slightly windward at the building height to measure the mean wind velocity. The natural frequencies and damping ratios from a preliminary study is shown in Fig. 10.

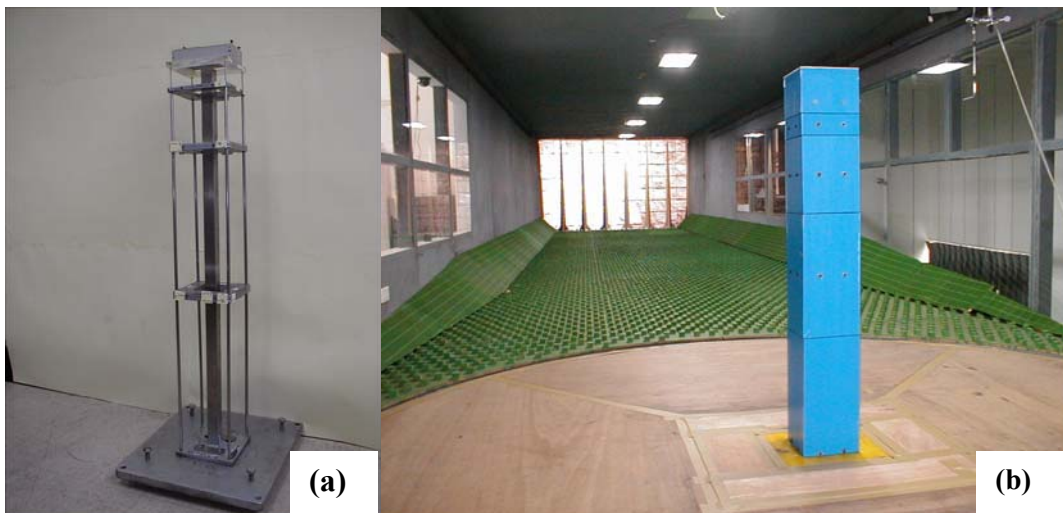


Fig. 9: (a) Frame Skeleton of the 1:300 Scaled High-rise Building Model;
(b) The Completed Building Model on the Boundary Layer Wind Tunnel

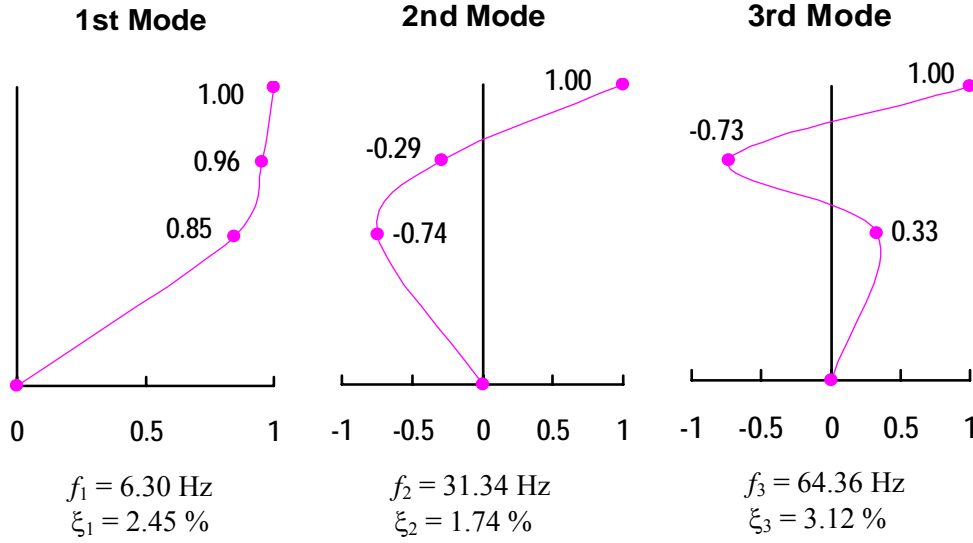


Fig.10: The First Three Modes of the Scaled Building

The AMD system installed on the top degree-of-freedom of the building is composed of a linear servomotor and a moving mass, as shown in Fig. 10. The mechanism of AMD system for generating active force to the structure is through the reaction inertial force of the moving mass. The movement of the moving mass on the linear motor is controlled by a conventional proportional-integral-derivative (PID) controller which aims to track the control command proportional to the absolute acceleration of the moving mass. During experiments, the building responses, i.e., the absolute displacements and absolute accelerations of all DOFs, the absolute acceleration of the moving mass of AMD system and the control command are recorded. The notation for the DOFs is numbered from the bottom to the top. Among them, the displacements and accelerations of the 1st, 2nd and 4th DOF are denoted as the controlled output vector $\mathbf{z} = [x_1, x_2, x_4, \ddot{x}_1, \ddot{x}_2, \ddot{x}_4]^T$ which is used in the identification and/or controller design. The measured output to be used as the feedback quantities is the absolute accelerations, i.e., $\mathbf{y} = [\ddot{x}_1, \ddot{x}_2, \ddot{x}_4]^T$. The sampling rate of the implemented controller is set to 1000 Hz.

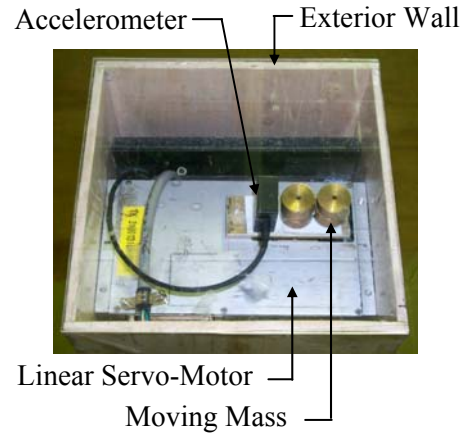


Fig. 11: Active Mass Driver System on the Top DOF

In the tests, the atmospheric boundary layer condition in the suburban area according to ANSI A58.1 (Terrain Classification B) is simulated in the wind tunnel, resulting in an atmospheric boundary layer with a gradient height of 400 m and power law exponent of the mean wind velocity equal to 0.23.

4.1 LQG Control Case

In this case, three filtered accelerations \ddot{x}_{1h} , \ddot{x}_{2h} , \ddot{x}_{4h} are also included in the controlled output vector \mathbf{z} . The inclusion of the three filtered accelerations in \mathbf{z} is to modulate the high frequency components in the acceleration, which may be possibly induced by active control. By following the design process proposed, the subsystem 1 and subsystem 2 are identified, respectively, and the results

are shown in Fig. 12. The subsystem 2 is identified at the mean wind velocity equal to 8.35m/s at the building height. It is noted that herein the subsystem 2 is identified under the assumption that the wind and structure may exist, and therefore the wind model in Fig. 4(a) is just an intermediate block that is never the concern in the process.

The effect of attack angle α is also investigated in this case. Since the characteristics in the along-wind ($\alpha=0^\circ$) and across-wind ($\alpha=90^\circ$) motions are quite different, the identification process of the subsystem 2 for these two situations is distinguished, as shown in Fig. 12 (b), (c).

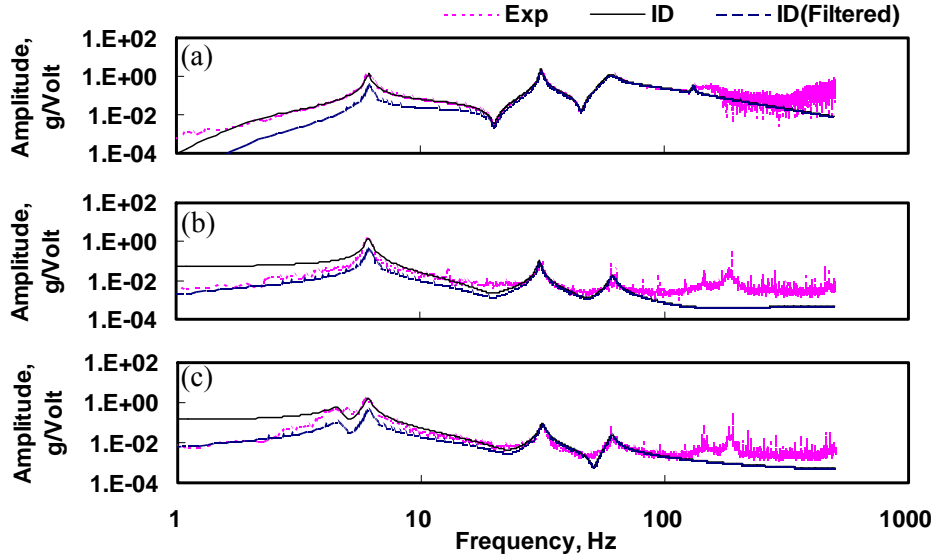


Fig.12: Amplitude of Transfer Function \ddot{x}_4 : (a) due to Actuator Command U ; (b) due to Along-wind Fictitious Load W ; (c) due to Across-Wind Fictitious Load W

For such a building with square cross-section, the observation from the experimental results shows that the vortex shedding effect becomes significant as the attack angle α is larger than 65° . Therefore, the LQG controller designed based on the nominal system of $\alpha=0^\circ$ (along-wind) is used for the cases $\alpha=0^\circ$, 30° and 45° , while that based on the nominal system of $\alpha=90^\circ$ (across-wind) is used for the cases $\alpha=70^\circ$ and 90° . These two LQG controllers are termed as the two-state gain scheduling controllers, and thus programmed in the computer in a way that proper switch can be carried on based on the attack angle.

Boundary layer wind tunnel tests of the actively controlled high-rise building subject to different wind attack angles are conducted under three different mean wind velocities of 7.13, 8.35 and 8.86 m/sec. The plots of displacement and acceleration of the 4th DOF (top floor) in temporal root-mean-square (rms) values for the cases of mean wind velocity equal to 7.13, 8.35 and 8.86 m/sec are presented as functions of the attack angle in Fig. 13 (a), (b) and (c), respectively. In Fig. 13, the four quadrants are used to illustrate different response quantities versus the attack angle: the 2nd and the 1st quadrants show the rms displacement of the 4th DOF and its reduction percentage w.r.t. the no control case, while the 3rd and 4th quadrants illustrate the rms acceleration of the 4th DOF and its reduction percentage w.r.t. the no control case.

As shown in Fig. 13, the performance of LQG control varies with the attack angle, however, the performance robustness is retained in resistance to the change of mean wind velocity. In the range of mean wind velocity considered here, the trend of control performance shows that the reduction is the best for the along-wind motion ($\alpha=0^\circ$) and gradually degraded to where the across-wind motion ($\alpha=90^\circ$) occurs. In the along-wind motion, the percentages of reduction of displacements and accelerations can achieve about 50%~60%, while those in the across-wind motion can only achieve about 30%~40%. Other detailed results can be found in [Wu et al. (2002a, 2002b, 2003a)].

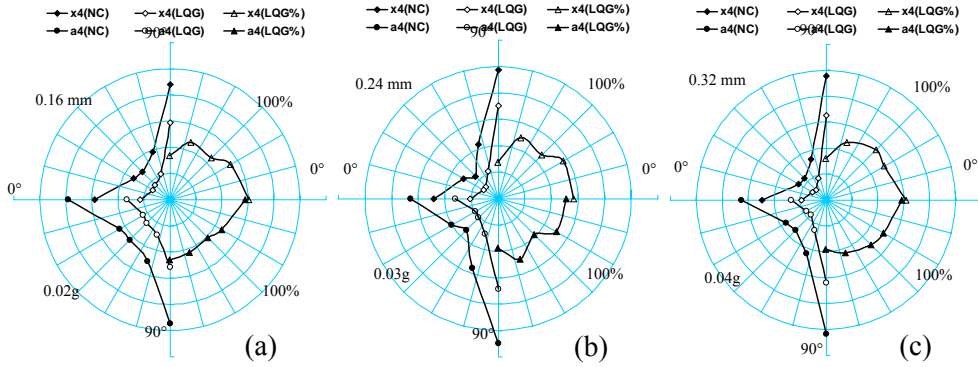


Fig. 13: Performance Diagram of Active Control under Different Attack Angle of Wind: (a) Wind Speed=7.13 m/s; (b) Wind Speed=8.35 m/s; (c) Wind Speed=8.86 m/s

4.2 H_{∞} Control Case

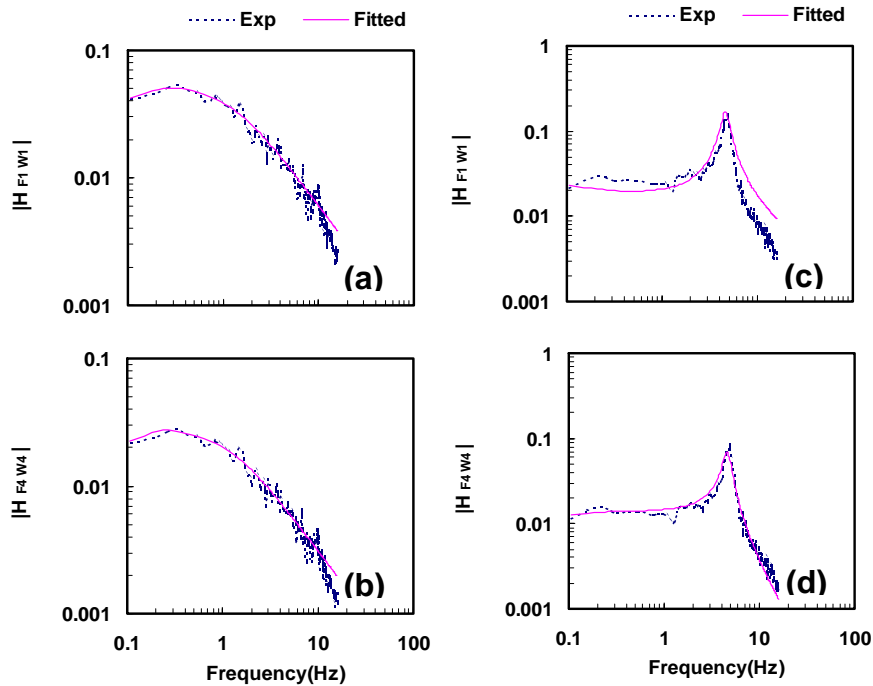


Fig. 14: Amplitudes of Transfer Functions of Spatially Completely Correlated Wind Loads versus Fictitious White Noise W under Mean Wind Speed 8 m/sec: (a), (b) Along-Wind Direction; (c), (d) Across-Wind Direction.

By following the design process proposed, the subsystem 1 and subsystem 2 are identified, respectively. The result of the subsystem 1 is similar to that shown in Fig. 12 (a). In this case, knowing that the aeroelasticity is not significant based on the previous study, the blocks of the building model and the structure contained in the subsystem 2 of Fig. 4 (a) are identified separately. The structure part is identified according to the data acquired in the process of the subsystem 1. The wind model part is constructed through the power spectrum of the base shear force acquired from the so-called high frequency force-balance test on a rigid building model with the same geometry at the mean wind speed 8 m/sec. By assuming a complete spatial correlation, the auto-power spectrum of

each wind force is estimated by portioning out the power spectrum of the base shear force following the distribution of the square of the mean wind velocity profile multiplied by the corresponding wind-acting area. Consequently the transfer functions of the wind model can be computed (shown in Fig. 14) and therefore its state equation can be obtained by curve-fitting these transfer functions. The detailed formulation in this regard is referred to [Wu *et al.* (2003b, 2006a)]

Table 1: Experimental Results of the LMI-Based H_∞ Controller

Mean Wind Speed = 8.0 m/sec					
(1)	DOF (2)	Along-wind		Across-wind	
		Peak (3)	R.M.S. (4)	Peak (5)	R.M.S. (6)
Displacement (mm)	1	0.1999 (44.77)	0.0394 (56.59)	0.5464 (45.48)	0.1396 (39.38)
	2	0.1346 (53.65)	0.0313 (60.86)	0.5037 (53.51)	0.1283 (41.07)
	4	0.1307 (50.19)	0.0282 (60.18)	0.4633 (57.81)	0.1155 (41.97)
Acceleration (g)	1	0.0321 (45.80)	0.0081 (48.02)	0.0825 (42.38)	0.0197 (43.05)
	2	0.0357 (43.48)	0.0079 (52.28)	0.0928 (40.23)	0.0204 (45.40)
	4	0.0326 (49.55)	0.0081 (51.84)	0.0871 (44.81)	0.0208 (46.05)
		Max(\ddot{x}_{md})=0.3121 g Max(U)=0.1410 Volt		Max(\ddot{x}_{md})=0.9975 g Max(U)=0.4493 Volt	
Mean Wind Speed = 8.8 m/sec					
(7)	DOF (8)	Along-wind		Across-wind	
		Peak (9)	R.M.S. (10)	Peak (11)	R.M.S. (12)
Displacement (mm)	1	0.2550 (44.67)	0.0544 (54.92)	0.7482 (45.48)	0.1968 (48.31)
	2	0.1963 (51.22)	0.0461 (58.31)	0.6786 (54.65)	0.1830 (51.01)
	4	0.1823 (51.13)	0.0420 (57.01)	0.6243 (59.72)	0.1649 (53.11)
Acceleration (g)	1	0.0535 (24.86)	0.0116 (43.54)	0.1182 (42.81)	0.0303 (48.81)
	2	0.0420 (46.59)	0.0114 (48.56)	0.1373 (39.65)	0.0316 (50.85)
	4	0.0442 (40.90)	0.0114 (49.06)	0.1275 (48.83)	0.0324 (51.29)
		Max(\ddot{x}_{md})=0.4284 g Max(U)=0.1948 Volt		Max(\ddot{x}_{md})=1.5860 g Max(U)=0.6530 Volt	

The application of H_∞ control follows the description in the section 2.3. The solution procedure of LMI-based approach used here is a simpler formulation presented by [Gahinet (1992)]. Then, the designed H_∞ controller is implemented on the high-rise building model and the wind tunnel tests are conducted under two different mean wind velocities of 8.0 and 8.8 m/sec at the building height. These velocities are equivalent to the reference wind velocities (at 10 m height) of 21.8 and 24 m/sec, respectively, for the full scale building in the suburban area with gradient height 400 m and power law exponent 0.23. Both the along-wind and across-wind loading are tested on the building to investigate the performance of active control in each direction.

The response quantities using the robust H_∞ controller are tabulated in Table 1; Columns (1)-(6) are for the case under mean wind speed of 8.0 m/sec while Columns (7)-(12) are for that under mean wind speed of 8.8 m/sec. In Table 1, the values inside the parentheses are the percentages of reduction with

respect to the responses without control. For further illustration, the time history plots of the controlled responses in 10 seconds (500 seconds in full scale) including the along-wind and across-wind motions are presented in Fig. 15. As shown in Table 1 and Fig. 15, the performance of the LMI-based H_∞ controller can achieve above 50% in reducing the peak and rms values of the displacement and accelerations in both the along-wind and across-wind directions. Other detailed results can be found in [Wu *et al.* (2002a), Wu *et al.* (2002b), Wu *et al.* (2005a)].

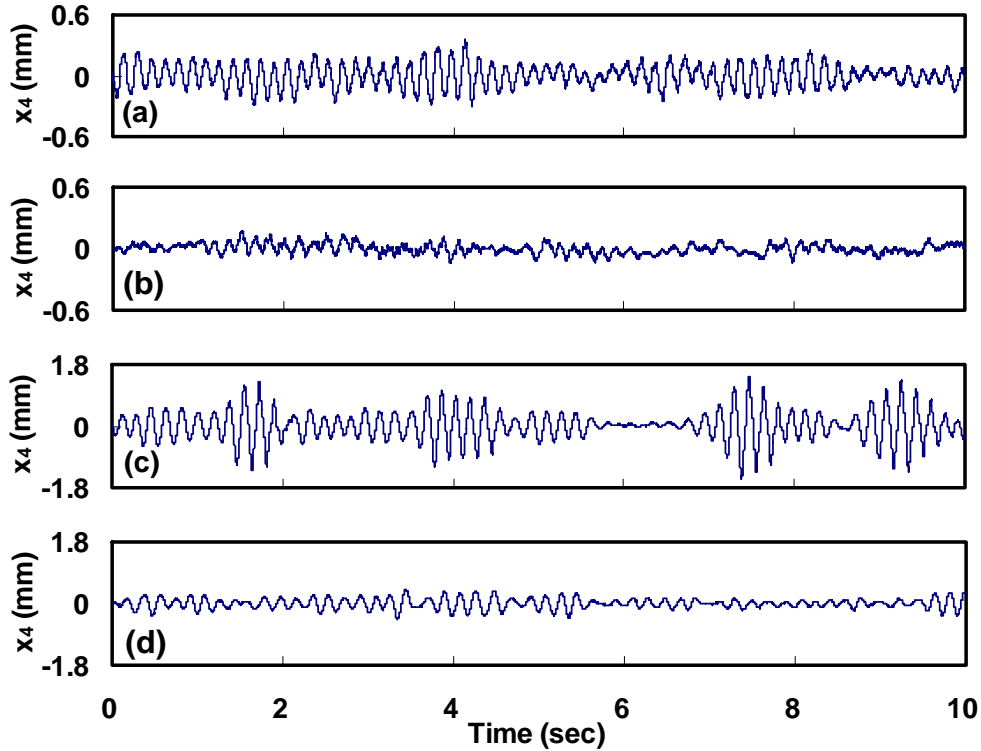


Fig. 15: Displacement Time Histories of the 4th DOF Using the Robust LMI-based Controller under Mean Wind Speed 8.8 m/sec: (a) Along-Wind Motion without Control; (b) Along-Wind Motion with Control; (c) Across-Wind Motion without Control; (d) Across-Wind Motion with Control.

5. IDENTIFICATION OF WIND-STRUCTURE INTERACTION BY ACTUATING DEVICES

The experiences gained from implementing actuators and the knowledge of using actuating devices have inspired the possible experimental study in the wind-structure interaction problems which some of our on-going projects are focusing on.

The conceptual idea is described as follows. By using the actuating device (for instance AMD) implemented on the structure, the responses of two situations, one is excited only by the actuating force (termed as actuating responses) while the other is excited by the smooth wind flow and actuating forces simultaneously (termed as total responses), can be measured and compared. Under the assumption that the structural behavior is linear to the excitation, the difference of the response in both situation is conceivably induced by the wind forces. If the wind-structure interaction is significant, the investigation of the dynamics between these wind forces and the total responses can be carried out to clarify the wind-structure interaction. The experimental and computational methodology is now under development for the identification of such relations.

Two on-going projects employing this concept are illustrated in the following. One example is shown in Fig. 16. The AMD actuating device is sequentially applied at the four indicated positions of a 1/160 high-rise building with lateral and torsional degrees of freedom to measure the responses mentioned

above. Shown in Fig. 17 is another example of bridge section model excited by a 2-axis actuating device in the heaving and pitching directions. The flutter derivatives are to be identified following the concept mentioned above. Some preliminary research results have been presented in [Wu *et al.* (2005b, 2006b)]



Fig. 16 : 1/160 Scaled Building Model Subject to the Actuating Force under Smooth Flow



Fig. 17 : Bridge Section Model Excited by a two-axis Actuating Device

6. CONCLUSIONS

This paper presents a general concept of a suitable design process that can take into account the possible control-structure interaction and wind-structure interaction for the active control application. Several important issues such as the identification scheme, construction of the nominal system, and requirements in the actuator specifications are addressed from the practical point of view. Advanced

control strategies, including the method of LQG (linear quadratic gaussian) and the idea of robust H_∞ control using LMI (linear matrix inequality) approach for an uncertain system, are introduced. The results of a successful implementation of using the active mass driver (AMD) system on a 1/300 scaled multiple-degree-of-freedom high-rise building model by wind tunnel tests are presented to demonstrate the applicability. Meanwhile, the experiences gained from implementing the actuators in the active control have also inspired the possibility of conducting experimental researches for the wind-structure interaction problems. The concept of using actuating device for the identification of wind-structure interaction is also briefly introduced.

7. REFERENCES

- Casciati, F (editor) (2002), *Proc. of Third World Conference on Structural Control*, John Wiley & Sons, N. Y.
- Chilali, M. and Gahinet, P. (1996), " H_∞ Design with Pole Placement Constraints : An LMI Approach", *IEEE Transactions on Automatic Control*, 41(3), pp. 358-367.
- Dyke, S.K., Spencer, Jr., B.F., Quast, P. and Sain, M.K. (1995), "The Role of Control-Structure Interaction in Protective System Design," *Journal of Engineering Mechanics, ASCE*, Vol. 121, No. 2, pp. 322-338.
- Dyke, S.K., Spencer, Jr. B. F., Quast P., Kaspari, Jr., D.C., and Sain, M.K. (1996), "Implementation of an Active Mass Driver Using Acceleration Feedback Control," *Microcomputers in Civil Engineering: Special Issue on Active and Hybrid Structural Control*, Vol. 11, pp. 305-323.
- Gahinet, P. (1992), "A Convex Parametrization of H_∞ Suboptimal Controllers", *IEEE Proceedings of the 31st Conference on Decision and Control*, pp. 937-942.
- Gahinet, P. and Apkarian, P. (1994), "A Linear Matrix Inequality Approach to H_∞ Control", *International Journal of Robust and Nonlinear Control*, 4, pp. 421-448.
- Housner, G. W., Masri, S. F. and Chassiakos, A. G. (editors) (1994), *Proc. of First World Conference on Structural Control*, USC, LA.
- Kobori, T., Inoue, Y., Seto, K., Iemura, H. and Nishitani, A. (editors) (1998), *Proc. of Second World Conference on Structural Control*, John Wiley & Sons, N. Y.
- Moore, B. C. (1981), "Principal Component Analysis in Linear System: Controllability, Observability and Model Reduction", *IEEE Transactions on Automatic Control*, Vol. 26, No. 1, pp. 17-32.
- Paraskevopoulos P. N. (1996), *Digital Control Systems*, Prentice Hall, NJ.
- Scherer, C., Gahinet, P. and Chilali, M. (1997), "Multiobjective Output-Feedback Control via LMI Optimization", *IEEE Transactions on Automatic Control*, 42(7), pp. 896-911.
- Simiu, E and Scanlan, R. H. (1996), *Wind Effects on Structures*, 3rd Edition, John Wiley & Sons.
- Wu, J. C. (2000), "Modeling of an Actively Braced Full-Scale Building Considering Control-Structure Interaction", *Earthquake Engineering and Structural Dynamics*, Vol. 29, No. 9, Sep., pp. 1325-1342.
- Wu, J. C. and Pan, B. C. (2002a), "Wind Tunnel Verification of Actively Controlled High-Rise Building in Along-Wind Motion", *Journal of Wind Engineering and Industrial Aerodynamics*, 90(12-15), 1933-1950.
- Wu, J. C. and Cheng, L. Y. (2002b), "Wind Tunnel Verification of Actively Controlled High-Rise Building under Varied Attack Angle of Wind", *Proceedings of Third World Conference on Structural Control*, Como, Italy, April 7-12.
- Wu, J. C., Leu W. C and Hsu, W. C. (2003), "Feasible Implementation of Robust Response Control for High-rise Building Using LMI-Based Approach", *Proceedings of 11th International Conference on Wind Engineering*, Lubbock, Texas, USA, June 2-5.
- Wu, J. C. and Cheng, L. Y. (2005a), "Effects of Attack Angle on Performance of Actively Controlled High-rise Building Motion", *Journal of Wind Engineering and Industrial Aerodynamics*, Vol. 93, No. 5, May, pp. 413-434.
- Wu, J. C. and Lin, S. W. (2005b), "Identification of Aero-elasticity of High-rise Buildings Using Forced Excitation", *Proceedings of Sixth Asia-Pacific Conference on Wind Engineering (APCWE-VI)*, Seoul, Korea, Sep. 12-14.

- Wu, J. C., Lu, W. C. and Hsu, W. C. (2006a), "Implementation of a Feasible Control Design Process Incorporating Robustness Criteria for Wind-Excited High-rise Buildings", *ASCE Journal of Structural Engineering*, Vol. 132, No. 1, Jan., pp. 89-101.
- Wu, J. C., Liu, W. C. and Juang, J. Y. (2006b), "Identification of Flutter Derivatives by Forced Vibration Technique", *Proceeding of Fourth International Symposium on Computational Wind Engineering (CWE2006)*, Yokohama, Japan, July 16-19.
- Zhou, K. and Doyle, J.C. (1998), *Essentials of Robust Control*, Prentice Hall.